# Asymmetric voltage attenuation in dendrites enables hierarchical heterosynaptic plasticity

**Toviah Moldwin[1], Menachem Kalmenson[2], Idan Segev[1,3]**

[1]Edmond and Lily Safra Center for Brain Sciences, [2]Faculty of Sciences and [3]Department of Neurobiology, the Hebrew University of Jerusalem, Jerusalem, Israel

**Correspondence:**
Toviah Moldwin
Toviah.moldwin@mail.huji.ac.il

**Keywords:** **Dendrites, Synaptic Plasticity, Cable models, Calcium, LTP, LTD, Heterosynaptic Plasticity, NMDA receptors, Voltage-gated channels, Long-term plasticity, Dendritic asymmetry**

# Abstract

Long-term synaptic plasticity has been shown to be mediated via calcium concentration ([$Ca^{2+}$]). Using a synaptic model which implements calcium-based long-term plasticity via two sources of $Ca^{2+}$, NMDA receptors and voltage-gated calcium channels (VGCCs), we show in dendritic cable simulations that the interplay between these two calcium sources can result in a diverse array of heterosynaptic effects. When spatially clustered synaptic input produces an NMDA spike, the resulting dendritic depolarization can activate VGCCs at other spines, resulting in heterosynaptic plasticity. Importantly, NMDA spike activation at a given dendritic location will tend to depolarize dendritic regions that are located distally to the input site more than dendritic sites that are proximal to it. This dendritic asymmetry results in a hierarchical heterosynaptic plasticity effect in branching dendrites, where clustered inputs to a proximal branch induce heterosynaptic plasticity primarily at branches that are distal to it. We also explore how simultaneously activated synaptic clusters located at different dendritic locations synergistically affect each other as well as the heterosynaptic plasticity of an inactive synapse "sandwiched" between them. We conclude that dendrites enable a sophisticated form of plastic supervision wherein NMDA spike induction can be spatially targeted to produce plasticity at specific dendritic regions.


# Introduction

The brain is believed to learn and store information via modifying the strengths of the synapses between neurons, a process known as long-term plasticity [1–6]. Experimentally, plasticity can be induced via a variety of stimulation protocols [4,5,7–11]. While some plasticity-inducing protocols such as spike-timing-dependent plasticity (STDP) require postsynaptic depolarization, in many cases it is possible to produce long-term potentiation (LTP) or long-term depression (LTD) via presynaptic stimulation alone (e.g. using high or low frequency stimulation, respectively), and some have argued that presynaptic inputs (without post synaptic response) are the primary driver of plasticity in the hippocampus [12–14] as well as in some cases in the cortex (Kumar et al., 2021).Over the past decades, since first proposed by John Lisman [16], evidence has mounted for a calcium-based theory of plasticity, known as the calcium control hypothesis [16–21]. In this framework, synapses change their strength depending on the calcium concentration ([$Ca^{2+}$]) at the postsynaptic dendritic spine. If the [$Ca^{2+}$] is low, no change occurs. If the [$Ca^{2+}$] rises above a critical threshold for depression ($\theta_D$), long-term depression (LTD) occurs and the synaptic strength is decreased. If the [$Ca^{2+}$] is above the critical threshold for potentiation ($\theta_P$), long-term potentiation (LTP) occurs and the synaptic strength is increased (Figure 1A). (It is usually assumed $\theta_P > \theta_D$ for cortical and hippocampal neurons [9,16], but the reverse may be true for cerebellar Purkinje cells [22,23]). It is believed that calcium promotes LTP via pathways involving protein kinases such as calmodulin kinase (CaMKII) [16,24–26], while promoting LTD via phosphatases such as calcineurin [16,27,28].

There are several sources of plasticity-inducing calcium at synapses. Two of the most prominent sources are the ligand- and voltage-gated NMDA receptor and the voltage gated calcium channel (VGCC). Experimentally-induced plasticity is disrupted or prevented when NMDA receptors or VGCCs are blocked, indicating that the calcium current through these sources is essential for long term plasticity [8,29–32]. Notably, internal calcium stores can also contribute to long term plasticity, see **Discussion**.)

One of the original motivations for the calcium-based plasticity theory [16,33] was the phenomenon of heterosynaptic plasticity – that sometimes, when a target synapse is subjected to a plasticity protocol, other synapses are affected as well (see [34,35] for reviews). For example, when LTP is induced at a target synapse, other synapses in the neuron can be depressed [36]. A calcium-based model can explain this phenomenon if the potentiating protocol produced a large [$Ca^{2+}$] influx (above $\theta_P$) in the target spine, and a smaller [$Ca^{2+}$] (above $\theta_D$ but below $\theta_P$) in non-target synapses. Lisman [33] proposed that this might happen in the following manner: when a target synapse is activated, such as by stimulating its presynaptic axons, NMDA receptors in the target spine are activated by the presynaptic glutamate, producing a calcium influx sufficient to induce homosynaptic potentiation at the synapse. In addition to increasing the [$Ca^{2+}$] in the target spine locally, the excitatory current also depolarizes the dendrite. If the depolarization is sufficient to activate VGCCs in other spines, they will also experience an influx of calcium, but smaller than that of the target spine, which has calcium both from NMDA receptors and VGCCs. If the calcium

concentration produced by the VGCCs is above $\theta_D$ but below $\theta_P$, the non-target synapses without NMDA activation will heterosynaptically depress (Figure 1C).

Heterosynaptic plasticity has also been shown to be spatially sensitive, with different plastic effects being observed at non-target synapses depending on where they are located relative to the target synapse. Some studies show heterosynaptic plasticity within short distances (~10 µm) from the target synapse [35,37,38], while other studies show heterosynaptic effects at up to 70 µm [39] or even from the basal to apical tree in hippocampal pyramidal neurons [36]. While the short range effects can be potentially be explained by molecular diffusion [35], it is unclear what the underlying principles are that determine the spatial spread of heterosynaptic plasticity over long distances, or what the functional significance of such heterosynaptic changes might be.

Another issue that arises under the calcium control hypothesis pertains to how simultaneous synaptic input at different regions of the dendrite affects plasticity. It is already known that NMDA synapses can interact synergistically with respect to depolarization—when multiple nearby synapses are activated simultaneously, the observed somatic EPSP is larger than the linear sum of the EPSPs generated when the synapses are activated separately, due to the voltage-dependence of the NMDA receptor [40]. However, it is less understood how simultaneous synaptic activity at different locations on the dendrite effect plastic changes at both activated and non-activated synapses.

Recently, a model synapse was developed as part of the Blue Brain Project [41] which incorporates NMDA receptors, VGCCs, and calcium-dependent long-term plasticity dynamics. This synapse model (with some modifications described in **Methods)** enables us to explore Lisman's hypothesis about the calcium basis of heterosynaptic plasticity in a cable model of a dendrite, which can provide insight into the spatial properties of heterosynaptic plasticity.

Because the soma of a neuron acts as a current sink, voltage attenuates more steeply toward the soma than away from it. This means that if an NMDA spike is activated locally in a dendrite, it will more strongly activate VGCCs at distal synapses than proximal synapses. We show that this can result in a hierarchical effect, where NMDA spike induction at a dendritic branch results in heterosynaptic plastic changes to synapses on its distal descendant branches. As such, branches that are more proximal to the soma can "supervise" synapses on all higher-order branching levels, whereas branches that are more distant from the soma have a more limited sphere of heterosynaptic influence.

We also perform simulations where an inactive spine is "sandwiched" between two different clusters on the dendritic tree in a "vertical" and "horizontal" configuration. We show that this results in a synergistic effect: $N$ synapses divided into two clusters at different dendritic locations will result in greater depolarization, and consequently more plasticity-inducing calcium influx, at the "sandwiched" spine than if all $N$ active synapses were placed in the same cluster.

Our study shows that local synaptic input can "supervise" plasticity in non-activated synapses and that this supervision effect depends on the dendritic branching structure. This means that synaptic plasticity operates in a more sophisticated manner than would be expected from simple presynaptic-postsynaptic models. Accordingly, a branching dendrite can be conceptualized as a hierarchical supervisory system for plasticity, where synaptic activity in proximal branches supervise synapses in distal branches. Moreover, multiple supervisors at different dendritic locations can interact synergistically to induce heterosynaptic plasticity at synapses located between them.

# Results

## Possible Heterosynaptic Effects

We begin by considering the range of possible heterosynaptic effects that may occur according to the hypothesis that homosynaptic plastic effects from presynaptic plasticity-induction protocols are induced by calcium from both NMDA receptors (which require presynaptic input and are amplified by postsynaptic depolarization) and VGCCs (which open in response to depolarization) while heterosynaptic effects are induced only via calcium influx to VGCCs responding to dendritic depolarization. On this view, an activated spine (i.e. a synapse that receives presynaptic input) will almost inevitably have a higher calcium concentration than non-activated synapses, as NMDA calcium conductance tends to be larger than VGCC conductance [42–45] and both the activated and non-activated synapses have VGCC conductance (Figure 1B). (We note that internal calcium stores can also contribute to synaptic [$Ca^{2+}$] and thereby affect both homosynaptic and heterosynaptic plasticity [37,46],

however the basic assumption that an activated spine will have a higher [$Ca^{2+}$] than a non-activated spine due the asymmetry in receptor activation will likely still hold in many cases; see Discussion for further details.)

Because calcium thresholds for LTP and LTD can vary from cell to cell [19], and can also be changed via meta-plastic processes [47], we generically map out several possible results that can occur to an activated and non-activated synapse given a few basic assumptions: A) an activated synapse has a higher calcium influx than a non-activated synapse B) plasticity thresholds and voltage-gated channel densities are approximately the same from spine to spine and C) that the calcium threshold for potentiation is higher than that of depression, i.e. $\theta_P > \theta_D$. We also disregard the magnitude of the plastic change and only consider the direction (potentiation or depression), as we assume that after inducing plasticity, synapses eventually drift toward a binary potentiated or depressed state, based on [48–50] (Figure 1A2-1A3).

Given these assumptions, the following plastic effects can result (Figure 1B): If the activated synapse is potentiated, non-activated synapses can also be potentiated (PP), but they can also be depressed (PD), or undergo no change (PN). If the activated synapse is depressed, non-activated synapses can also be depressed (DD) or undergo no change (DN). If the activated synapse does not change, neither will the non-activated synapse (NN). Given assumptions our assumptions above, the following possibilities are *not* possible: DP, NP, and ND (Figure 1C). (In the event that $\theta_D > \theta_P$, as in Purkinje cells, the allowed possibilities are PP, PN, DP, DD, DN, NN, and the disallowed possibilities are PD, NP, and ND, however the simulations used in this study assume $\theta_P > \theta_D$ to match known results from the hippocampus and cortex [18,20]. We also assume that the input to the activated synapse is not sufficiently large to put it into a post-potentiative neutral zone where the calcium concentration is so high that potentiation mechanisms are inactivated, see [51]).

Intuitively, given values for $\theta_D$ and $\theta_P$, homosynaptic effects from presynaptic input protocols will vary based on the “strength” of synaptic input (e.g. input frequency or cluster size, as we use here). Strong inputs can potentiate the synapse, medium strength inputs can depress it, and weak inputs will induce no change. As heterosynaptic effects are mediated by dendritic depolarization, heterosynaptic effects will also depend on the input strength to the activated synapse, in addition to other factors which determine the “spillover effect” of the activated synapse’s dendritic depolarization on non-active synapses.

One important factor that may affect heterosynaptic effects is the distance of the non-activated synapse from the activated synapse. Because voltage attenuates with distance in a dendrite [52,53], non-activated synapses that are closer to the activated synapse will see more dendritic depolarization and are thus likely to have a larger calcium influx through VGCCs than those that are further away. This effect can potentially give rise to a Mexican hat phenomenon [34]—for non-activated synapses close to an activated synapse, the dendrite might be sufficiently depolarized locally to enable an influx of calcium through the VGCCs that surpasses $\theta_P$, resulting in potentiation. Synapses that are somewhat further out will see attenuated voltage, possibly enabling a calcium influx which crosses $\theta_D$ but not $\theta_P$. And non-activated synapses that are sufficiently far from the activated synapse will only see a highly attenuated voltage trace which is insufficient to generate a calcium influx above $\theta_D$.

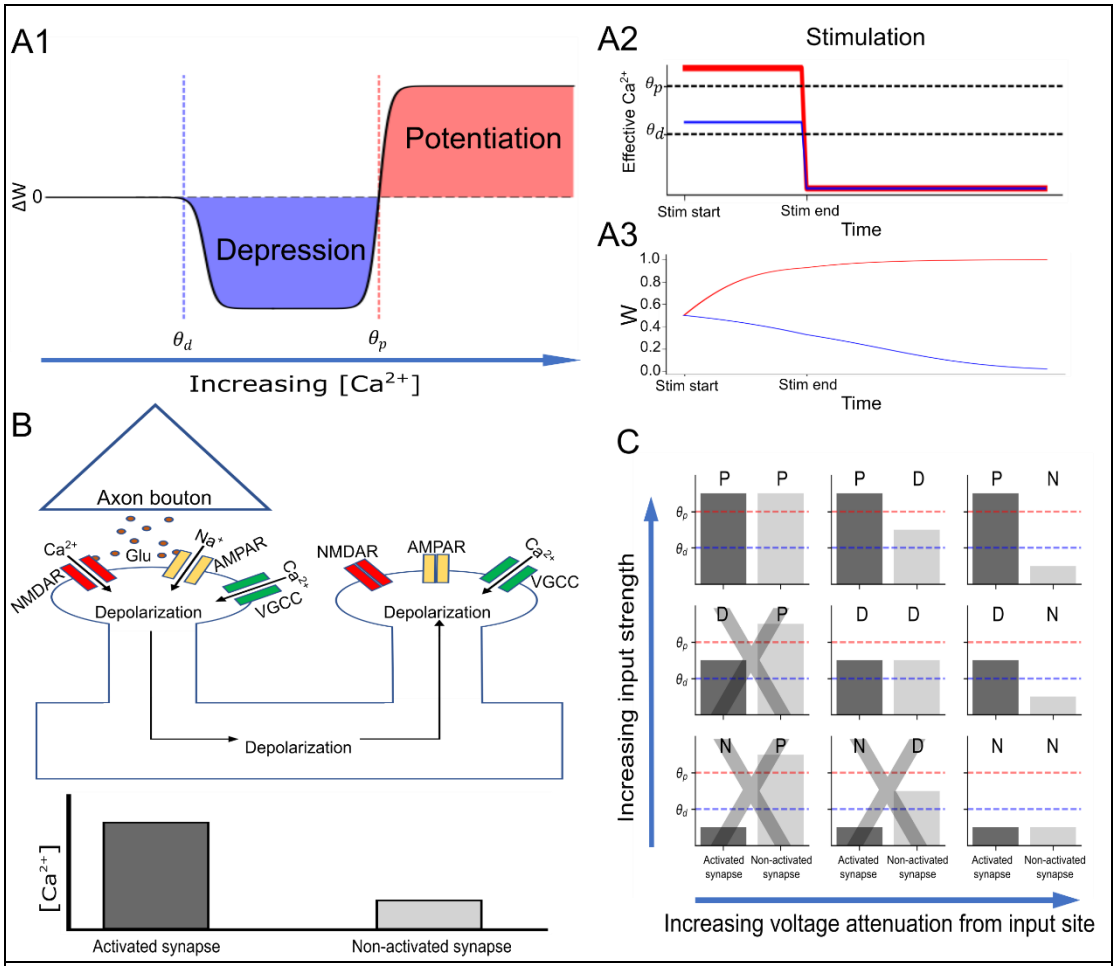


**Figure 1. Induction of homosynaptic and heterosynaptic plasticity with NMDA receptors and VGCCs**.

(**A1**) Calcium control hypothesis. When the [$Ca^{2+}$] crosses the depression threshold $\theta_D$, the synapse is weakened. When the [$Ca^{2+}$] crosses the potentiation threshold $\theta_P$, the synapse is strengthened. (**A2)** Example [$Ca^{2+}$] stimulation to illustrate dynamics of the Graupner-Brunel plasticity rule. Synaptic [$Ca^{2+}$] is raised to either a depressive (blue line) or potentiative (red line) level for several minutes and then reduced to baseline. (**A3)** Plasticity dynamics weight over time due to the [$Ca^{2+}$] stimulation from A2. While [$Ca^{2+}$] is elevated, the synapse either potentiates or depresses (red and blue lines, corresponding to red and blue lines from **A2**). When the [$Ca^{2+}$] stimulus ends, the synapse slowly drifts to a binary UP or DOWN state depending on its weight. (Panels A2-A3 produced by Li Azran). (**B**) VGCC hypothesis for heterosynaptic plasticity. Presynaptic input induces $Ca^{2+}$ influx through the NMDA receptors as well as the VGCCs (due to the depolarization of the spine), resulting in a high [$Ca^{2+}$] for inducing homosynaptic plasticity (black bar, bottom). The resultant dendritic depolarization can open VGCCs at other spines, resulting in a lower [$Ca^{2+}$] for inducing heterosynaptic plasticity. (**C**) Schematic diagram of how input strength (e.g. cluster size) and attenuation (e.g. as a function of distance) can affect homosynaptic and heterosynaptic effects. As input strength increases, the homosynaptic effect at the activated synapse goes from no change (N) to depression (D) to potentiation (P); as attenuation increases, the heterosynaptic effect will decrease from potentiation to depression to no change. Given the assumption that the heterosynaptic [$Ca^{2+}$] is always less than the homosynaptic [$Ca^{2+}$], some possibilities (marked with a gray X) are impossible.

## Voltage attenuates asymmetrically in dendrites

The distance-dependent attenuation description of heterosynaptic plasticity is complicated by the fact that voltage attenuation in the dendrite is highly asymmetric. In most neurons the soma acts as a current “sink”, due to the fact that it is connected to many dendrites, which provide many more paths for current to travel when moving toward the soma versus away from it. This fact is captured in the asymmetry of the transfer resistance between proximal and distal points on the dendrite (Supplementary 1).

To demonstrate the effects of distance and transfer resistance on voltage attenuation, we created a ball-and-stick cable model of a single dendrite 200 μm long attached to a soma (Figure 2A). We enlarged the diameter of the soma to replicate the electrical sink effect that would occur in a neuron with a full dendritic morphology, based on the layer 5 pyramidal cell model from (Hay et al., 2011) (see Methods, Supplementary 1). We placed a cluster of 5 spines with excitatory synapses at 100 μm from the soma. We also placed non-activated spines at 60 μm and 200 μm from the soma in order to record from the spine heads. We simultaneously activated all synapses in the cluster at 100 μm with a single presynaptic spike and recorded the local voltage at the soma, every segment of the dendrite, and at the heads of both the activated and non-activated spines. Voltage attenuated from the heads of the activated spines to the spine base, but almost no attenuation was visible from the base of the activated spines at 100 μm to the head of the non-active spine at 200 μm. By contrast, the voltage attenuated substantially from the base of the activated spines at 100 μm to the base of the non-active spine at 60 μm.

We replicated this experiment with a cluster of 18 synapses at 100 μm, which was sufficient to create an NMDA spike. (We note that it is possible to create an NMDA spike with fewer clustered synapses if the synapses are activated at a high frequency [55,56]. In this and subsequent simulations, for simplicity, we vary only the number of synapses and use a single presynaptic spike at each cluster to create an NMDA spike; cluster size here thus serves as a convenient single-variable measure of input strength.) The same asymmetric effect was qualitatively observed; voltage attenuation was very minor from the activation site to the distal tip and very substantial from the activation site toward the soma (Figure 2B-C).

We then demonstrate how the asymmetric attenuation plays out in a branching dendrite model. We created a branching dendritic tree with 4 branch levels and attached it to a somatic compartment (compensated as described above). We activated a cluster of 18 synapses in the middle of a branch at the third level from the soma, generating a local NMDA spike. The NMDA spike propagated to the daughter branches of the activated branch with minimal attenuation, propagated to the sister branches of the activated branch and their daughter branches with mild attenuation, and propagated to the rest of the dendritic tree with substantial attenuation (Figure 2D). The stark contrast in the depolarization magnitude of different regions of the dendritic tree in response to an NMDA spike raises the possibility that asymmetric attenuation may play some functional role in governing how different parts of the dendrite communicate with each other.

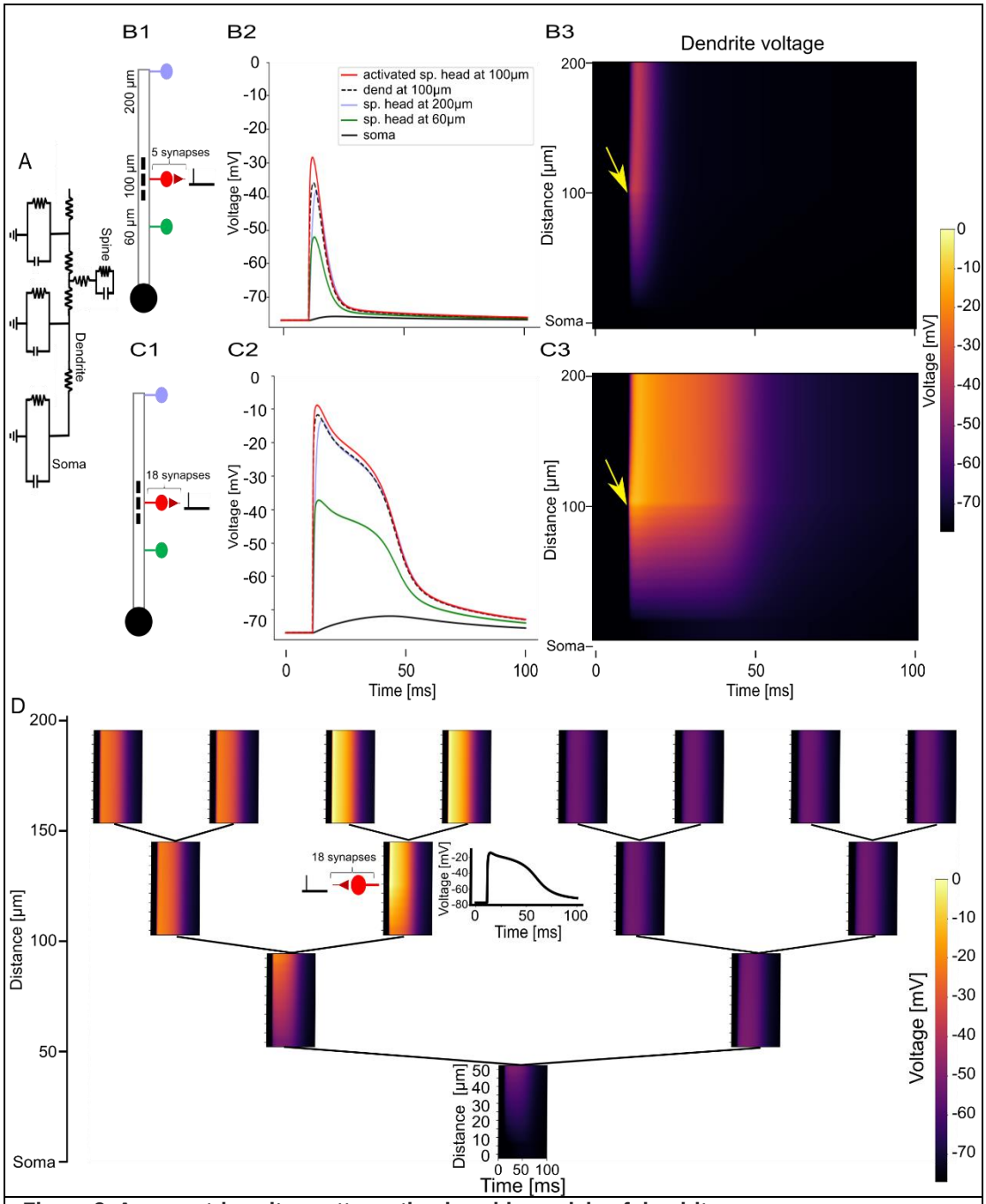


**Figure 2. Asymmetric voltage attenuation in cable models of dendrites**

(**A**) Circuit diagram of a ball and stick dendrite model with spines. (**B1**) Experiment schematic. A cluster of 5 synapses at 100 µm from the soma are simultaneously activated with a single presynaptic spike. Voltages are recorded from one of the activated spine heads (red spine), the activated spine base (black dashed line), a non-activated spine at 200 µm (blue spine), a non-activated spine at 60 µm (green spine) and the soma (black solid circle). (**B2**) Voltage traces from recording sites depicted in B1. Voltage is highest at the activated spine head (red solid line) and attenuates somewhat to the spine base (dashed black line). Virtually no attenuation occurs from the activated spine base to the distal spine head (blue), but significant attenuation is seen toward the proximal spine (green line) and the soma (black line). (**B3**) Voltage recordings at every segment of the dendrite during the experiment depicted in B1. Color depicts dendritic voltage as a function of time (horizontal axis) and distance from soma (vertical axis). Arrow indicates time and location of the activated synaptic cluster. (**C1-C3**) Same as B1-B3 except a cluster of 18 synapses are simultaneously activated to generate an NMDA spike. (**D**) Dendritic voltage heatmaps in each branch of a 4-level branching dendrite model in response to an NMDA spike initiated via activating a cluster of 18 synapses at the indicated dendritic location. Dendritic branches are depolarized to different magnitudes depending on where they are relative to the input location. Inset: voltage trace at the base of the activated cluster.

1

## Asymmetric attenuation produces asymmetric heterosynaptic plasticity

We now show how asymmetric voltage attenuation can impact heterosynaptic plasticity according to the hypothesis that heterosynaptic plasticity is induced via via voltage gated calcium channels (VGCCs). We placed a spine at each segment of the ball and stick model (one spine every 10 μm) and activated a cluster of 27 synapses at the center of the dendrite (100 μm). This produced a large NMDA spike at the activated spines, depolarizing the dendrite sufficiently to open VGCCs at non-activated spines on the dendrite.

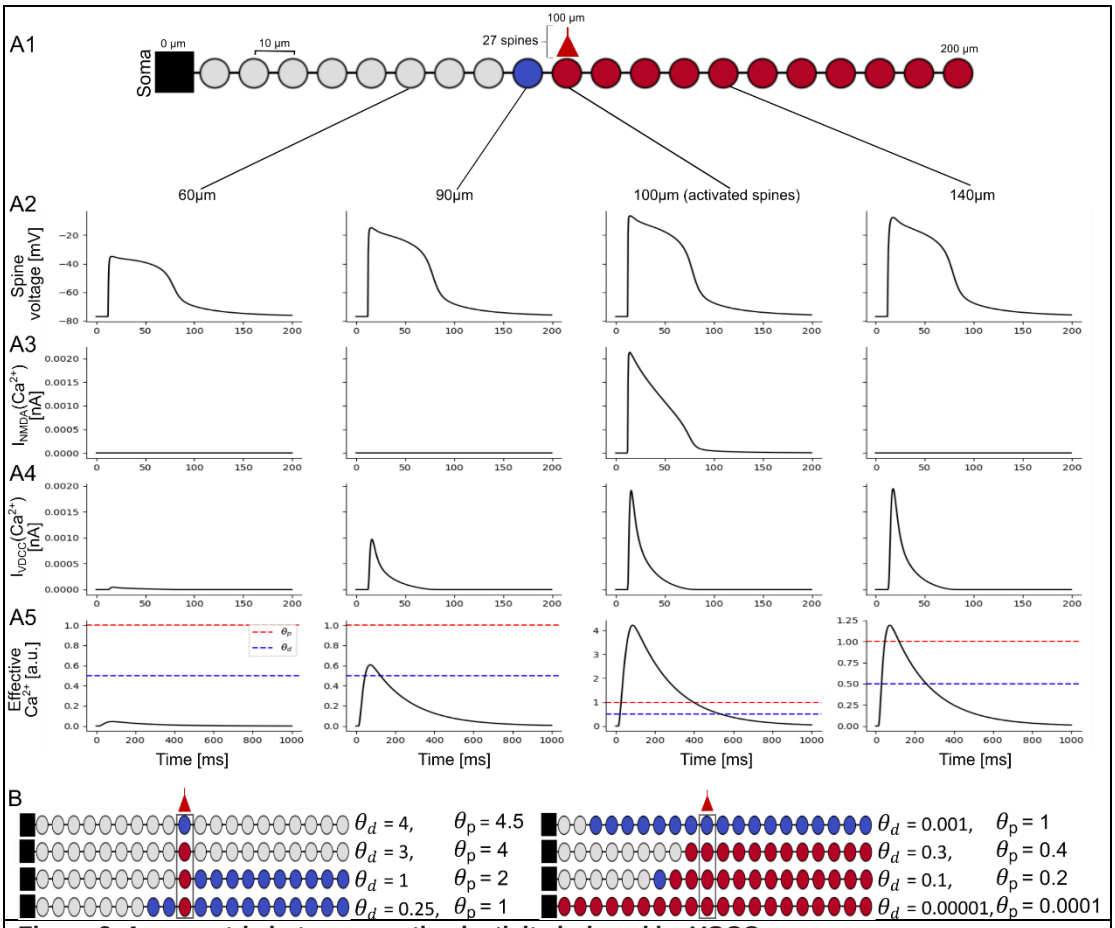


**Figure 3. Asymmetric heterosynaptic plasticity induced by VGCCs**
**(A1)** Top**:** A ball and stick model dendrite with spines (circles) placed every 10 μm. A cluster of 27 spines (shown as a single circle with an input) is activated at the center of the dendrite (100 μm), generating an NMDA spike which results in homosynaptic and heterosynaptic plasticity. The activated spines and the spines distal to it are potentiated (red), the spine 10 μm proximal to the activated spine is depressed (blue), and the other proximal spines do not change (gray). (**A2**) Spine head voltage traces shown at 60 μm, 90 μm, 100 μm (exemplar activated spine), and 140 μm. The NMDA spike is seen at all spines, but the voltage at the proximal location (60 μm) is substantially attenuated. (**A3**) $Ca^{2+}$ current through the NMDA receptor at the 4 depicted spines. Only the activated spine has NMDA current because NMDA receptors are ligand gated. (**A4**) $Ca^{2+}$ current through the VGCCs at the depicted spines; $Ca^{2+}$ current depends on local voltage (from A2). (**A5**) Effective [$Ca^{2+}$] (as accumulated by the $Ca^{2+}$ integrator) at the depicted spines. At 60 μm the [$Ca^{2+}$] is below $\theta_D$ (blue dashed line) so no change occurs, at 90 μm, the [$Ca^{2+}$] reaches above $\theta_D$ but below $\theta_P$ (red dashed line) so depression occurs, at 100 μm and at 140 μm the [$Ca^{2+}$] reaches above $\theta_P$ so the synapses are potentiated. (**B**) As in A1 (27 synapses activated at 100 μm) but with different calcium thresholds, resulting in different heterosynaptic effects.

At the active site, both NMDA and VGCCs brought substantial amounts of calcium current into the cell, allowing the calcium accumulator (i.e. the effective calcium used for plasticity in the plastic synapse model of [41] to surpass $\theta_P$, generating homosynaptic potentiation. At spines distal to the input site (i.e. from 100 μm to 200 μm), the voltage from the dendritic depolarization was sufficient for the VGCCs to bring in enough calcium current to also induce heterosynaptic potentiation. However, at a spine 10 μm proximal to the input site (90 μm,from the soma) the voltage had already attenuated sufficiently such that the VGCCs only brought in enough calcium to induce depression. At 20 μm proximal to the input site, (80 μm from the soma) the voltage had already attenuated sufficiently such that the calcium from the VGCCs was insufficient to cross $\theta_D$, so all other proximal spines were left unchanged (Figure 3A). Of

course, these results hold true only for the specific calcium thresholds for plasticity used in our simulation; different calcium thresholds can yield a variety of different effects when performing the same experiment. Nevertheless, the general rule holds that, all else being equal, it is easier to induce heterosynaptic plasticity between the input site and the distal dip than to induce heterosynaptic plasticity on-path to the soma (Figure 3B).

This spatial asymmetry in heterosynaptic effects is especially pronounced when considering a branching dendrite. Asymmetric attenuation from an input site can create branch-dependent dendritic depolarization. To demonstrate this effect, we placed spines every 10 μm on the four-layer branched model described above. In separate experiments, we activated clusters of 20, 30, 40, or 50 synapses at each of the four branch levels and observed the plastic changes at all spines on the dendritic tree (Figure 4).

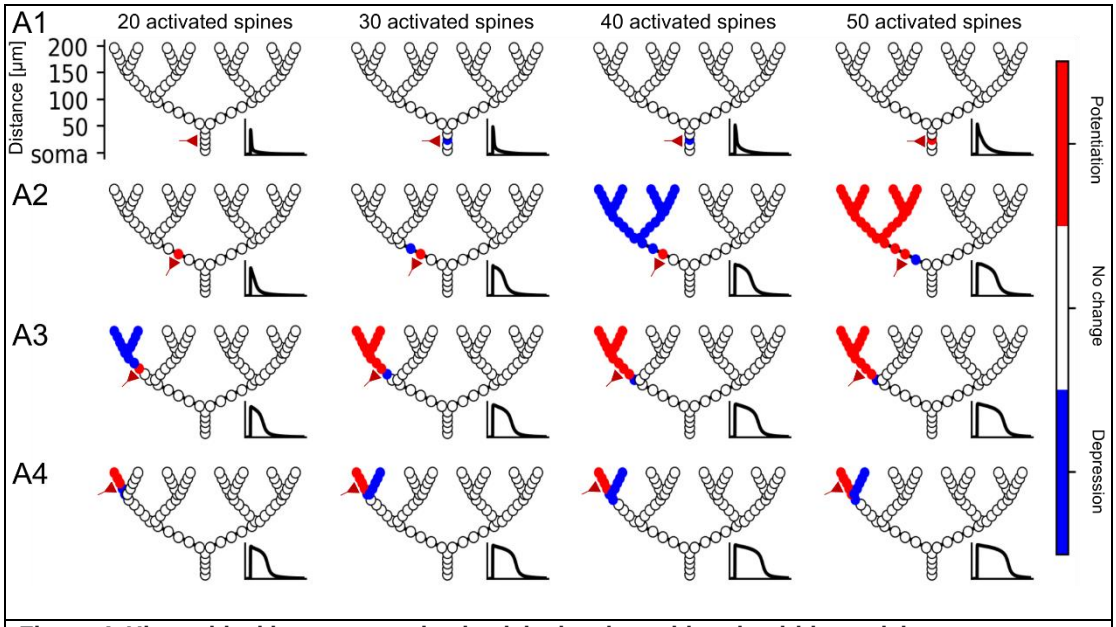


**Figure 4. Hierarchical heterosynaptic plasticity in a branching dendritic model**
**(A1)** A synaptic cluster of 20 (first column), 30 (second column), 40 (third column), or 50 (fourth column) spines is simultaneously activated at the middle of the proximal branch. Inset: spine head voltage at activated site. Due to the low input resistance at the proximal branch, no NMDA spike is generated, so only homosynaptic plasticity is observed at the input site. **(A2-A4)** As in A1, but the cluster of activated is now placed at the second, third, or fourth branching level. When the input is sufficiently strong, an NMDA spike is generated and heterosynaptic plasticity is observed.

If the synaptic cluster is placed on the branch most proximal to the soma, due to the low input resistance, it is difficult to induce an NMDA spike or homosynaptic plasticity (30 spines are required for depression, 50 for potentiation). Even 50 synapses are insufficient in this model to produce an NMDA spike at the most proximal branch, and thus heterosynaptic plasticity is not induced. If we move the cluster up to the second branching level, homosynaptic potentiation is induced with 20 synapses, and it becomes possible to produce an NMDA spike with 30 synapses, and we observe heterosynaptic depression of the dendritic tree distal to the input site when 40 spines are activated, which turns into potentiation when 50 spines are activated. At the third branching level, 20 synapses is already sufficient to produce an NMDA spike and heterosynaptic depression at dendritic spines distal to the input site, and 30 spines turns the heterosynaptic depression to potentiation. At the fourth branching level, the input resistance is sufficiently high to cause both homosynaptic and heterosynaptic potentiation at spines distal to the input site with 20 synapses, and with 30 synapses the voltage manages to propagate sufficiently in the proximal direction to depress the input site's sister branches.

The tiered nature of heterosynaptic plasticity in a dendrite, where input to a more proximal branch can induce heterosynaptic plasticity at branches that are distal to it, suggests that dendritic branches might supervise each other in a hierarchical manner. Branches that are closer to the soma (although not so close that it is difficult to generate an NMDA spike) can "teach" the branches that are distal to it via the backwards propagation of the NMDA spike, leading to heterosynaptic potentiation or depression in descendant branches. Moreover, distal branches with low input resistances may be able to supervise their sibling

branches via a competitive process where an input sufficient to depress the branch with homosynaptic input will heterosynaptic depress synapses on a sibling branch.

## Synergistic Synaptic Sandwiching

Until now, we have only looked at heterosynaptic effects produced by the activation of a single cluster of co-localized spines, generating a single NMDA spike. It is possible that multiple clusters may be activated simultaneously, generating diverse depolarization effects in the dendritic tree. From a plasticity standpoint, it is important to think about how the clusters of activated synapses can affect each other (through both VGCC and NMDA-dependent activations) as well as how they affect inactive synapses via heterosynaptic plasticity (through VGCC activation). While it is not feasible to explore the full combinatorial space of cluster activations, we consider a canonical case in the ball-and-stick model where an inactive synapse, placed 130 μm from the soma, is “sandwiched” in between two spine clusters, one toward the proximal end of the dendrite (60 μm) and one at the distal end of the dendrite (200 μm). This case is important for heterosynaptic plasticity because it illustrates the tradeoff between two principles: On the one hand, voltage attenuates more toward the soma than away from it. On the other hand, it is easier to generate a large NMDA spike at distal synapses, due to the higher input resistance at more distal locations.

To illustrate this tradeoff, suppose we have 40 active synapses to distribute between the proximal cluster and the distal cluster with the goal of maximizing the depolarization, and thus the heterosynaptic calcium influx, at the centrally located inactive synapse. If the input resistance effect dominates, it would be better to place all synapses distally. If the asymmetric transfer resistance effect dominates, we should assign all 40 synapses to the proximal cluster. In fact, however, it seems that the answer lies in between these two extremes: Placing 20 synapses each at the proximal and distal location results in a slightly larger depolarization at the heterosynaptic synapse than placing all 40 synapses together in a single cluster at either the proximal or distal location (Figure 5A-B). The synergy between distal and proximal clusters is not restricted to the case of 40 synapses; for any given number of synapses there appears to be a “sweet spot” for distributing those synapses between the proximal and distal locations to maximize heterosynaptic effects at the central location, albeit with a tendency to assign more synapses to the proximal location (Figure 5C-D).

The increased depolarization when the synapses are divided in separate clusters can be explained by the fact that there are diminishing returns for placing additional synapses at the same location, due to the reduced driving force when the dendrite is depolarized to near its reversal potential. It is thus better to separate the synapses into separate clusters at locations that are somewhat electrically separated to avoid “wasting” synapses on a dendritic segment that is already maximally depolarized. (Additional synapses can still increase the *duration* of an NMDA spike when the branch is depolarized to near its electrical reversal, however for the purposes of heterosynaptic plasticity it is often crucial to maximize the peak voltage at the heterosynaptic synapse in to ensure that the peak calcium through the VGCCs passes the plasticity thresholds. The duration above the plasticity thresholds also affects the magnitude of the plastic changes in the early phase of long-term plasticity, but in the bistable Graupner-Brunel bistable model, magnitude information is lost after several hours in the late phase of plasticity when the synaptic weights are stabilized into a binary UP/DOWN state, see (Graupner & Brunel, 2012).)

The benefit of dividing synapses into two groups is not observed at the proximal and distal locations themselves. While active proximal synapses do increase calcium influx at distal synapses and vice versa (due to both NMDA and VGCC voltage-dependence), to maximize peak calcium influx at proximal spines, it is best to put all the synapses proximally, and to maximize peak calcium influx at distal spines, it’s best to put all the synapses distally (Figure 5C-D).

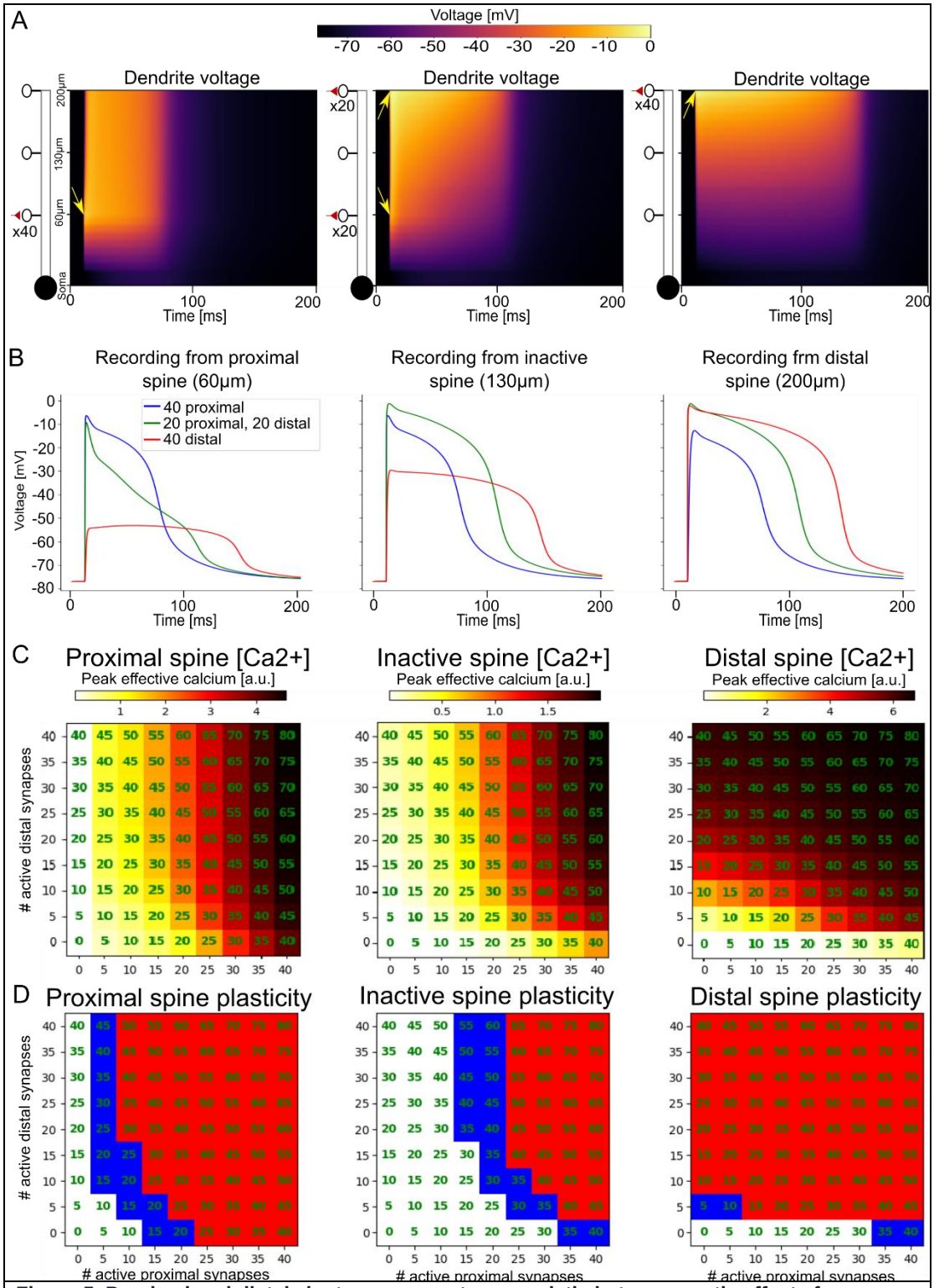


**Figure 5. Proximal and distal clusters can create synergistic heterosynaptic effects for "sandwiched" synapses.**

**(A)** Dendritic voltage over time in a ball-and-stick model when 40 synapses are placed proximally (left) distally (right) or distributed evenly between the proximal and distal locations (center). Arrows show activation locations and times. (**B)** Spine head voltage recordings from a proximal activated spine (left), the central non-activated spine (center), and a distal activated spine (right) for the 3 cases shown in A. **(C)** Peak calcium influx at the proximal (left), central (middle), or distal spine (right) as a heatmap, for different numbers of spines placed in the distal and proximal clusters. Annotations indicate total number of spines (proximal + distal). **(D)** Plastic effect (red: potentiation, blue: depression, white: no change) due to the calcium influx from (C).

The synergistic heterosynaptic sandwiching effect also pertains in a branched neuron model. We placed varying numbers of activated spines on a proximal branch (second layer)

and a distal branch (fourth layer) in our 4-layer branched model to observe the heterosynaptic effects at a non-activated spine on the central branch (third layer). As in the ball-and stick model, the peak calcium at the non-active, central spine was maximized when active synapses were distributed between the proximal and distal branch (Figure 6A-C, Supplementary Figure S2).

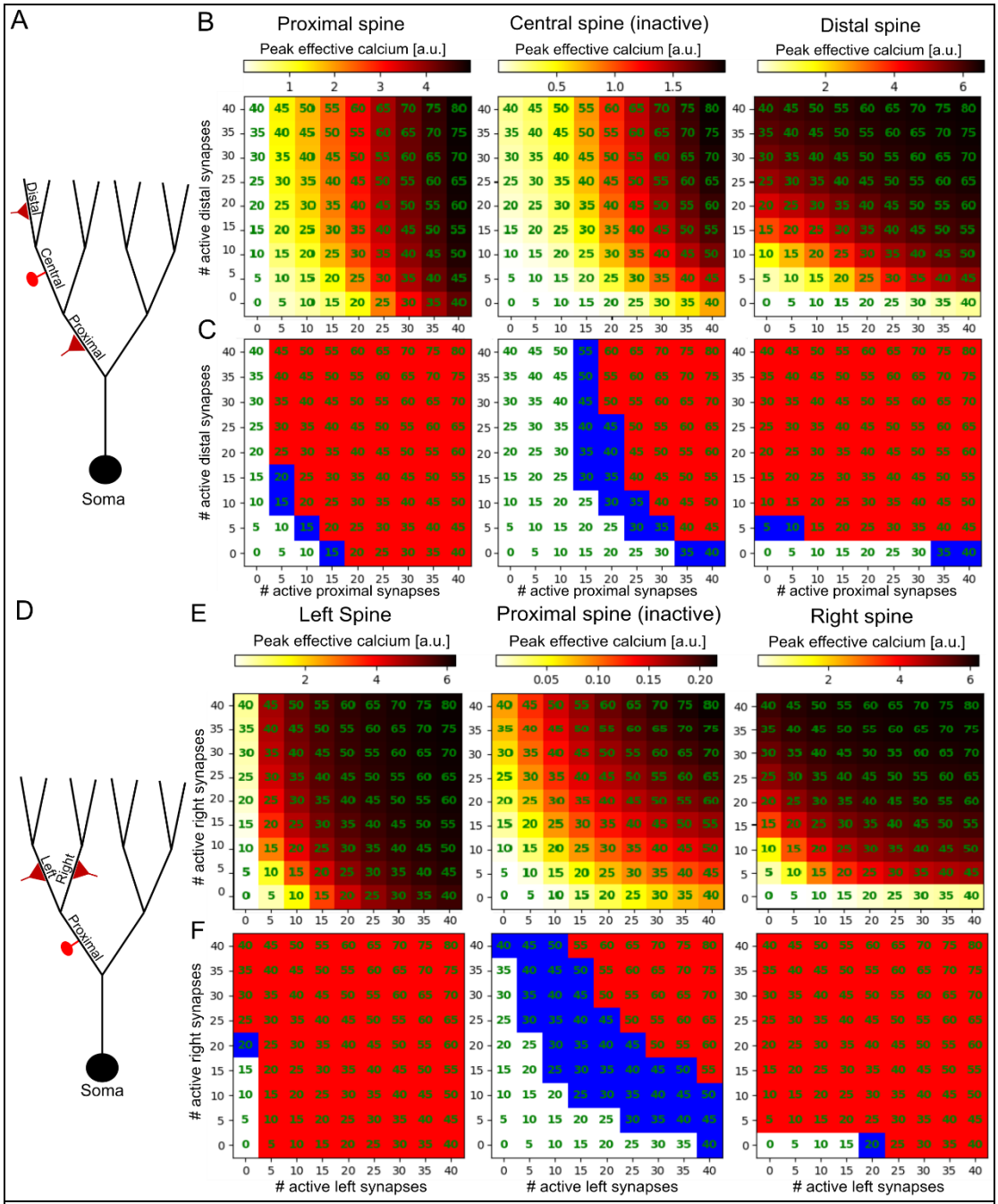


**Figure 6. Vertical heterosynaptic sandwiching in a branched model**
**(A)** Experiment schematic for vertical sandwiching in a branched model. Clusters of spines are activated at proximal (2nd layer) and distal (4th layer) branches to observe the effect on non-activated spine on each other and on synapse place on a central branch (3rd layer) **(B)** Peak calcium at an exemplar spine on the proximal (left), central (middle) or distal (right) branches, as in Figure 5C. **(C)** Plastic effect on each spine as a function of cluster sizes (red: potentiation, blue: depression, white: no change). **(D)** Experiment schematic for horizontal sandwiching in a branched model. Clusters of spines are activated at the left and right branches to explore the effect on each other and a non-activated synapse on the parent branch. **(E-F)** Calcium and plasticity for the horizontal sandwiching experiment **a**s in **C-D.** See Supplementary Figures S2 and S3 for voltage traces and heatmaps.

In additional to this “vertical sandwiching” scenario, we also explore a “horizontal sandwiching” case, where an inactive spine is placed in the middle of a branch at the second branching layer, and varying numbers of active synapses are placed at its left and right daughter branches at the third branching layer. (Because we are trying to induce heterosynaptic plasticity from a distal input to a proximal location, it is necessary here to lower the calcium thresholds, see **Methods**.) We again observe in this context that from the perspective of the inactive spine on the proximal parent branch, dividing the active spines between the left and right daughter branches tends to maximize the peak calcium available for producing heterosynaptic plasticity. As we would expect from the symmetry of the left and right branches relative to the parent branch, the peak heterosynaptic calcium tends to be maximal when the left and right branches have the same number of activated spines (Figure 6D-F, Supplementary Figure S3).

We have thus shown that when an inactive synapse is placed between two synaptic clusters, whether it is “vertically sandwiched” between a distal and proximal branch or “horizontally sandwiched” between two of its daughter branches, plasticity-inducing calcium influx tends to be greater than if all the active synapses were placed in a single cluster. This raises the possibility that in addition to the hierarchical supervision effect we showed above, it may be possible to engineer synapse placement in a sophisticated manner to maximize heterosynaptic plasticity induction without requiring an excessive number of active synapses at the same location.

## Discussion

Our simulations have shown a wide range of consequences that arise from the hypothesis that heterosynaptic plasticity can result from dendritic depolarization-induced calcium influx through VGCCs. Despite using a very simple cable model of a dendrite, model synapses with NMDA channels, VGCCs, and a simple calcium-based plasticity mechanism were sufficient to produce spatially-sensitive heterosynaptic effects. Specifically, we have demonstrated that a strong dendritic input which generates an NMDA spike can induce heterosynaptic plasticity at dendritic sites that are distal to it due to asymmetric voltage attenuation toward the soma. This asymmetry can create a hierarchical heterosynaptic effect in a branching dendrite structure, where strong inputs to proximal branches can act as a “supervisors” to synapses on more distal branches. Moreover, when two clusters of inputs are active, each cluster can increase the plasticity-inducing calcium influx at spines the other cluster as well as non-active spines. As we showed in the “sandwiching” experiments, plasticity-inducing calcium influx to a non-active spine can be maximized by dividing spines into two clusters, rather than placing all spines at the same location.

The extent to which these phenomena occur in biology remains an open question, and we encourage experimentalists to use the predictions of our model to design experiments to test whether these hierarchical heterosynaptic plastic effects indeed occur in the brain. If our predictions here are borne out by experiments, heterosynaptic plasticity can produce a more sophisticated form of plasticity than those that consider only presynaptic and postsynaptic firing (such as frequency-dependent plasticity or spike-timing dependent plasticity). If dendritic NMDA spikes indeed act as heterosynaptic supervisors for other spines on the dendrite, the dendritic branching structure and the location of NMDA spike induction become essential to the implementation and functional consequences of neural plasticity. Location-sensitive NMDA spike-dependent plasticity rules are particularly critical in light of findings that backpropagating somatic action potentials may not reach distal synapses for the purpose of plasticity induction, while NMDA spikes can induce plasticity at distal synapses [15].

Further work can explore diverse neuronal types with different dendritic morphologies to examine whether the branching structure of different neurons may lend themselves to different kinds of plasticity computations. For example, the elaborate fractal branching structure of Purkinje neurons may lend those neurons to be optimized for segregated hierarchical units, while neurons with long, branching dendrites (such as apical dendrites of L2/3 cells) may exhibit more attenuation in the proximal-distal direction and thus behave less hierarchically, as descendant branches themselves can act as electrical sinks relative to the parent branch if there is sufficient surface area in the descendant branches [57].

The branch-dependent variation of heterosynaptic plasticity we show in our model is in line with the theory that the dendritic branch may be a fundamental computational unit in the neuron (Branco & Häusser, 2010). Consistent with the idea that neurons can behave as a

two-layer neural network [58,60], hierarchical plasticity can potentially serve as a biophysical basis for a multi-layer learning algorithm within a single neuron, perhaps akin to the backpropagation algorithm in deep neural networks in feed-forward artificial neural networks (Jones & Kording, 2021; Rumelhart et al., 1986). The details of how such an algorithm would operate remain an open avenue for investigation.

The hierarchical plasticity story is complicated somewhat by our “sandwiching” results, which demonstrate that, for a given number of synapses, heterosynaptic effects can be maximized by distributing them into two spatially segregated clusters instead of placing them all at the same location. This points to the possibility of an even more sophisticated supervision scheme, where multiple synaptic clusters can be strategically placed at different dendritic locations to produce spatially targeted heterosynaptic plasticity. Spatiotemporally-targeted inhibition may also help shape the spread of heterosynaptic plasticity. Further experimental and theoretical work could explore these possibilities in more detail. In any event, the diverse heterosynaptic effects we have shown here provide support for the claim that neurons may behave as complex nonlinear units [60,62,63] as opposed to simple perceptrons where synapses are modified independently [64]. Moreover, the pronounced asymmetrical results observed in our simulations indicate that computational models which make use of distance-dependent NMDA superlinearities (e.g. [65,66]) should take into account branching structure and absolute synaptic location in addition to the relative distance of synapses from each other.

## Additional biological considerations

Our model, in line with the proposal of Lisman [33], assumes that the only medium of communication between active and inactive synapses is dendritic voltage depolarization, which can activates VGCCs of other synapses on the dendrite. We note that many other mechanisms for the induction of heterosynaptic plasticity have been suggested (See [34,35] for reviews). One alternative possibility is that calcium itself diffuses from one synapse to another, however experimental evidence suggests that calcium diffusion from the spine head into the dendritic shaft is negligible [67]. Other molecules have also been implicated in inducing heterosynaptic effects, such as h-Ras, Rac1, RhoA, Arc, BDNF-TrkB, CaMKII and calcineurin [35,38], however these molecules have only been shown to diffuse up to 10µm along the dendrite, while heterosynaptic effects have been shown to occur at much larger distances between activated and non-activated synapses [36,39]. As such, the depolarization-based model remains an important candidate mechanism of heterosynaptic plasticity; future work incorporating more detailed molecular effects can build on the results we present here. It may be that there are different short-distance and long-distance heterosynaptic effects, with short-distance effects occurring via molecular mechanisms such as local CamKII and Calcneurin activity, while long-distance effects may be due to the voltage mechanism we describe here.

Regarding the fidelity of the parameters our simulation to biological reality, there are several questions that would require additional experimental evidence and more detailed models to fully confirm. Our calcium channel model assumed a single type of calcium channel, and we chose a conductance value that roughly corresponds to what might expect as the aggregate conductance of all high voltage-activated VGCCs. A more precise model that includes all forms of VGCCs with their appropriate unitary conductances, kinetics, and densities would allow for greater precision in our claims. Additionally, the kinetics of calcium accumulation and the plasticity thresholds for calcium used here could be better constrained with more experimental evidence. We also assumed that calcium channel density and plasticity thresholds were the same from spine to spine; in biology these may differ on a spine-by-spine basis even with a single neuron. Moreover, the spatial effects we observed in our simulations assume a passive dendritic cable; active mechanisms in biological dendrites such as voltage-gated sodium and potassium channels have been shown to differentially modulate voltage propagation in different neurons (Golding et al., 2001), so these mechanisms would consequently be expected to modify the spatial dynamics of heterosynaptic plasticity as well.

Inhibitory synapses also likely play an important role in the spatial reach of heterosynaptic plasticity. Inhibition can have different consequences for the neuronal voltage depending on the location of the inhibitory synapses [69–71] as well as their timing relative to excitatory NMDA inputs [72]. As such, spatiotemporally targeted inhibition can be used to

modulate the heterosynaptic effects we describe here, enabling a bidirectional control system for heterosynaptic plasticity.

Several studies have shown that internal calcium stores play an important role in both homosynaptic and heterosynaptic plasticity [37,46,73–76]. Ryanodine and $IP_3$ receptors in the endoplasmic reticulum enable calcium-induced calcium release (CICR), which can affect plasticity in a variety of ways. Although experimental results regarding the role of CICR are more subtle than the model we have presented here, one way to think about CICR is as an amplifier of calcium coming from NMDA and voltage gated calcium channels. As such, assuming that CICR increases monotonically with calcium from extracellular sources, the basic qualitative principle that activated synapses will experience more calcium release than non-activated synapses due to NMDA receptor activation still holds, but it may shift the homosynaptic and heterosynaptic effects observed (e.g. from DN to PD, see figure 1C).

There is also evidence that the effect of internal calcium stores is highly localized into micro domains and depends on various second messengers, resulting in a more complex picture of homosynaptic and heterosynaptic effects [76]. Moreover, recent experimental evidence suggests that CICR can enhance the spatial spread of calcium activity in dendrites, potentially enhancing plasticity [77]. Understanding the relationship between voltage-dependent and CICR-dependent mechanisms of heterosynaptic plasticity is an important avenue of future investigation.

Another biological mechanism that may affect the plastic results we predict here are small-conductance $Ca^{2+}$-activated K+channels (SK channels). SK channels can repolarize the cellular membrane in response to calcium influx [51,78,79], potentially reducing both homosynaptic and heterosynaptic effects.

One additional crucial biological question is whether the early stage heterosynaptic plasticity induced by calcium influx is stabilized into late-term plasticity via protein synthesis, which has been shown to be necessary to make plastic changes last longer than an hour [49,80,81]. One recent study [82], showed that plasticity-induced protein synthesis may primarily occur within 3 µm of a potentiated synapses, suggested that heterosynaptic effects may not necessarily be long-lived. However, it is possible that a very strong clustered stimulation, such as we described here, may induce protein synthesis at more distant locations.

## Methods

Simulations were done using NEURON with a Python wrapper [83,84]. Code was written using Python 3.7.6 and NERUON version 7.7.2. Figures were made with the Matplotlib package.

Model parameters can be found in Table 1. The dendrite models were largely based on the layer 5 pyramidal cell model of [54] except where described otherwise in Table 1. The dendritic axial resistance and diameter were chosen such as to fit with empirically described results [85]and to ensure that a robust NMDA spike could be obtained with ~20 synapses [86]The ball and stick model had a dendrite 200 µm, composed of 50 electrical segments (cylinders). The branched model had 4 levels of bifurcating branches. Each branch was 50 µm long and was composed of 10 segments.

To create a ball and stick model that replicates the electrical sink effect observed in the soma of a neuron with a full complement of extended dendrites, we expanded the diameter of the ball-and-stick soma such as to have the same input resistance by applying the formula $R_N = \frac{R_m}{A}$ , where $R_N$ is the somatic input resistance of the full layer 5 pyramidal cell model in units of $\Omega$, $R_m$ is the membrane resistivity in units of $\Omega cm^2$, and $A$ is the area of the compensated soma in units of $cm^2$, resulting in a compensated soma diameter of 718 µm. See Supplementary 1A for a comparison of transfer resistances between the fully pyramidal model and our ball-and-stick model.

As in the Hay model, effective dendritic membrane resistivity $\mathrm{dendritic}\ R_m$ is divided by two to compensate for the surface area of (unmodeled) spines and dendritic membrane capacitance $\mathrm{dendritic}\ C_m$ was doubled to ensure that the membrane time constant $\tau$ does not change.

*Table 1*

| **Model parameters** | | | |
|---|---|---|---|
| | **Property** | **Value** | **Reference** |
| **Electrical parameters** | $R_a$ | Soma: 100 Ωcm | |
| | | Dend: 150 Ωcm | |
| | $C_m$ | Soma: 1 μF/cm$^2$ | [54] |
| | | Dendrite: 1*2 = 2 μF/cm$^2$ | [54] |
| | $E_{pas}$ | -77 mV | Based on resting potential of [54] |
| | $R_m$ | Soma: 30 KΩcm$^2$ | [54] |
| | | Dendrite: 44/2* = 22 KΩcm$^2$ | [54] |
| | $g_{max}$ | AMPAR (INITIAL): 1.5 nS<br>AMPAR (UP): 2 nS<br>AMPAR (DOWN): 1 nS | [87] |
| | | VGCC: 20 pS | [42–44] |
| | | NMDAR: 1.31 nS | [45] |
| **Morphological parameters** | Diameter | Dendrite: 0.75 μm | [88] |
| | | Soma: 718 μm | Fit to match [54] |
| | Length | Dendrite (ball and stick): 200 μm | |
| | | Dendrite branch (branched model): 50 μm | |
| | | Soma: 23 μm | [54] |
| **Spine parameters** | $R_a$ | 150 Ωcm | |
| | $R_m$ | 10.7 KΩcm$^2$ | [54]<br>(no spine comp.) |
| | Diameter | Head: 0.4 μm | [89] |
| | | Neck: 0.07 μm | Arellano et al. 2007a (fit to ensure $R_{neck}$ of 226.6 MΩ) |
| | Length | Neck: 0.66 μm | Arellano et al. 2007a |
| | $R_{neck}$ | Neck: 226.6 MΩ | [90] |

* Rm divided by 2 and $C_m$ multiplied by 2 to compensate for surface area of unmodeled spines while maintaining the membrane time constant

For synapses, we used the Blue Brain Project's synapse model with NMDA receptors, VGCCs, and calcium-based long-term plasticity model [41]; details of the synaptic and calcium dynamics can be found there. The calcium-based plasticity model itself is based on [48].

We made several modifications to the Blue Brain synapse: (1) We initialized the synapses in a neutral state of 1.5 nS (equivalent to $\rho = 0.5$ , i.e. the unstable fixed point in the Graupner-Brunel model), so synapses could be easily depressed or potentiated when the calcium accumulator crossed the plasticity thresholds. (2) We changed the maximum

conductance of the NMDA receptor (gmax_NMDA) to 1.31 nS based on [45] (3) We increased the unitary conductance of the VGCCs to 20 pS based on [42–44]. While the kinetics of the VGCC model are based on the R-type VGCC, 20 pS was chosen as a rough estimate of the total unitary conductance over all high-voltage activated channels. (4) We modified the equations for total spine calcium conductance and concentration to account for the fact that we were explicitly modeling the spine as a cylinder with the parameters in Table 1.

Except where indicated, for Figures 3-6, plasticity thresholds for the [$Ca^{2+}$] were: $\theta_D = 0.5$, $\theta_P = 1$. For Figure 7, plasticity thresholds were $\theta_D = 0.2$, $\theta_P = 0.4$. Plasticity thresholds can vary from cell to cell, so all plasticity results presented here should be taken as qualitative illustrations of possible plastic effects rather than specific quantitative predictions.


## Acknowledgements

The authors would like to thank András Ecker and Giuseppe Chindemi for the use of their plastic synapse model [41], their support and helpful discussions in dealing with technical and conceptual issues over the course of this project, and for their helpful comments our manuscript. We also thank Yuri Rodrigues and Thomas Chater for their thorough comments on the manuscript. Thanks to Li Azran for panels 1A2-1A3 illustrating the dynamics of the Graupner-Brunel plasticity rule.


## References


1. Nabavi S, Fox R, Proulx CD, Lin JY, Tsien RY, Malinow R. Engineering a memory with LTD and LTP. Nature. 2014;511: 348–352. doi:10.1038/nature13294
2. Humeau Y, Choquet D. The next generation of approaches to investigate the link between synaptic plasticity and learning. Nature Neuroscience 2019 22:10. 2019;22: 1536–1543. doi:10.1038/s41593-019-0480-6
3. Hebb D. The organization of behavior. A neuropsychological theory. 1949 [cited 9 Sep 2021]. Available: https://pure.mpg.de/rest/items/item_2346268/component/file_2346267/content
4. Bliss T, Lomo T. Long-lasting potentiation of synaptic transmission in the dentate area of the anaesthetized rabbit following stimulation of the perforant path. The Journal of Physiology. 1973;232: 331–356. doi:10.1113/jphysiol.1973.sp010273
5. Bliss T, Collingridge G. A synaptic model of memory: long-term potentiation in the hippocampus. Nature. 1993;361: 31–39. doi:10.1038/361031a0
6. Whitlock J, Heynen A, Shuler M, Bear M. Learning induces long-term potentiation in the hippocampus. Science (1979). 2006;313: 1093–1097.
7. Shouval HZ, Wang SSH-H, Wittenberg GM. Spike timing dependent plasticity: A consequence of more fundamental learning rules. Frontiers in Computational Neuroscience. 2010;4: 19. doi:10.3389/fncom.2010.00019
8. Bi G, Poo M. Synaptic Modifications in Cultured Hippocampal Neurons: Dependence on Spike Timing, Synaptic Strength, and Postsynaptic Cell Type. Journal of Neuroscience. 1998;18: 10464–10472. doi:10.1523/JNEUROSCI.18-24-10464.1998
9. Artola A, Bröcher S, Singer W. Different voltage-dependent thresholds for inducing long-term depression and long-term potentiation in slices of rat visual cortex. Nature. 1990;347: 69–72. doi:10.1038/347069A0
10. Rose GM, Dunwiddie T v. Induction of hippocampal long-term potentiation using physiologically patterned stimulation. Neuroscience Letters. 1986;69: 244–248. doi:10.1016/0304-3940(86)90487-8
11. O'Connor DH, Wittenberg GM, Wang SS-H. Dissection of Bidirectional Synaptic Plasticity Into Saturable Unidirectional Processes. Journal of Neurophysiology. 2005;94: 1565–1573. doi:10.1152/jn.00047.2005
12. White G, Levy WB, Steward O. Evidence that associative interactions between synapses during the induction of long-term potentiation occur within local dendritic domains. Proceedings of the National Academy of Sciences. 1988;85: 2368–2372. doi:10.1073/PNAS.85.7.2368
13. Hardie J, Spruston N. Synaptic Depolarization Is More Effective than Back-Propagating Action Potentials during Induction of Associative Long-Term Potentiation

in Hippocampal Pyramidal Neurons. Journal of Neuroscience. 2009;29: 3233–3241. doi:10.1523/JNEUROSCI.6000-08.2009

14. Lisman J, Spruston N. Postsynaptic depolarization requirements for LTP and LTD: a critique of spike timing-dependent plasticity. Nature Neuroscience. 2005;8: 839–841. doi:10.1038/nn0705-839

15. Kumar A, Barkai E, Schiller J. Plasticity of olfactory bulb inputs mediated by dendritic NMDA-spikes in rodent piriform cortex. Elife. 2021;10. doi:10.7554/ELIFE.70383

16. Lisman J. A mechanism for the Hebb and the anti-Hebb processes underlying learning and memory. Proceedings of the National Academy of Sciences. 1989;86: 9574–9578. doi:10.1073/pnas.86.23.9574

17. Shouval HZ, Bear MF, Cooper LN. A unified model of NMDA receptor-dependent bidirectional synaptic plasticity. Proceedings of the National Academy of Sciences. 2002;99: 10831–10836. doi:10.1073/PNAS.152343099

18. Cho K, Aggleton JP, Brown MW, Bashir ZI. An experimental test of the role of postsynaptic calcium levels in determining synaptic strength using perirhinal cortex of rat. The Journal of Physiology. 2001;532: 459. doi:10.1111/J.1469-7793.2001.0459F.X

19. Yang S, Tang Y, Zucker RS, Yang S-N, Tang Y-G, Zucker Selective RS. Selective Induction of LTP and LTD by Postsynaptic [Ca 2 ] i Elevation. 1999.

20. Mulkey RM, Malenka RC. Mechanisms underlying induction of homosynaptic long-term depression in area CA1 of the hippocampus. Neuron. 1992;9: 967–975. doi:10.1016/0896-6273(92)90248-C

21. Cummings JA, Mulkey RM, Nicoll RA, Malenka RC, JA C, RM M, et al. Ca2+ signaling requirements for long-term depression in the hippocampus. Neuron. 1996;16: 825–833. doi:10.1016/S0896-6273(00)80102-6

22. Piochon C, Titley HK, Simmons DH, Grasselli G, Elgersma Y, Hansel C. Calcium threshold shift enables frequency-independent control of plasticity by an instructive signal. 2016; 13221–13226. Available: https://www.pnas.org/content/113/46/13221

23. Coesmans M, Weber JT, de Zeeuw CI, Hansel C. Bidirectional Parallel Fiber Plasticity in the Cerebellum under Climbing Fiber Control. Neuron. 2004;44: 691–700. doi:10.1016/j.neuron.2004.10.031

24. Neveu D, Zucker RSRS. Postsynaptic Levels of [Ca2+]i Needed to Trigger LTD and LTP. Neuron. 1996;16: 619–629. doi:10.1016/S0896-6273(00)80081-1

25. Malenka RC, Kauer JA, Perkel DJ, Mauk MD, Kelly PT, Nicoll RA, et al. An essential role for postsynaptic calmodulin and protein kinase activity in long-term potentiation. 1989;340: 554–557. Available: https://www.nature.com/articles/340554a0

26. Malinow R, Schulman H, Tsien RW. Inhibition of Postsynaptic PKC or CaMKII Blocks Induction But Not Expression of LTP. Science (1979). 1989;245: 862–866. doi:10.1126/science.2549638

27. Mulkey RM, Herron CE, Malenka RC. An Essential Role for Protein Phosphatases in Hippocampal Long-Term Depression. Science (1979). 1993;261: 1051–1055. doi:10.1126/science.8394601

28. Mulkey RM, Endo S, Shenolikar S, Malenka RC. Involvement of a calcineurin/inhibitor-1 phosphatase cascade in hippocampal long-term depression. Nature 1994 369:6480. 1994;369: 486–488. doi:10.1038/369486a0

29. Dudek SM, Bear MF. Homosynaptic long-term depression in area CA1 of hippocampus and effects of N-methyl-D-aspartate receptor blockade. Proceedings of the National Academy of Sciences. 1992;89: 4363–4367. doi:10.1073/pnas.89.10.4363

30. Fino E, Paille V, Cui Y, Morera-Herreras T, Deniau J-M, Venance L. Distinct coincidence detectors govern the corticostriatal spike timing-dependent plasticity. J Physiol. 2010;588: 3045–3062. doi:10.1113/jphysiol.2010.188466

31. Shindou T, Ochi-Shindou M, Wickens JR. A Ca2+ Threshold for Induction of Spike-Timing-Dependent Depression in the Mouse Striatum. Journal of Neuroscience. 2011;31: 13015–13022. doi:10.1523/JNEUROSCI.3206-11.2011

32. Golding NL, Staff NP, Spruston N. Dendritic spikes as a mechanism for cooperative long-term potentiation. Nature. 2002;418: 326–331. doi:10.1038/nature00854

33. Lisman JE. Three Ca2+ levels affect plasticity differently: the LTP zone, the LTD zone and no man’s land. The Journal of Physiology. 2001;532: 285–285. doi:10.1111/J.1469-7793.2001.0285F.X

34. Chistiakova M, Bannon NM, Bazhenov M, Volgushev M. Heterosynaptic Plasticity. The Neuroscientist. 2014;20: 483–498. doi:10.1177/1073858414529829
35. Chater TE, Goda Y. My Neighbour Hetero — deconstructing the mechanisms underlying heterosynaptic plasticity. Current Opinion in Neurobiology. 2021;67: 106–114. doi:10.1016/J.CONB.2020.10.007
36. Lynch GS, Dunwiddie T, Gribkoff V. Heterosynaptic depression: a postsynaptic correlate of long-term potentiation. Nature. 1977;266: 737–739. doi:10.1038/266737a0
37. Royer S, Paré D. Conservation of total syanptic wight through balanced synaptic depression and potentiation. Nature. 2003;422: 518–522. doi:10.1038/nature01532.1.
38. Tong R, Chater TE, Emptage NJ, Goda Y. Heterosynaptic cross-talk of pre- and postsynaptic strengths along segments of dendrites. Cell Reports. 2021;34: 108693. doi:10.1016/J.CELREP.2021.108693
39. Engert F, Bonhoeffer T. Synapse specificity of long-term potentiation breaks down at short distances. Nature. 1997;388: 279–284. doi:10.1038/40870
40. Polsky A, Mel BW, Schiller J. Computational subunits in thin dendrites of pyramidal cells. Nat Neurosci. 2004;7: 621–7. doi:10.1038/nn1253
41. Chindemi G, Abdellah M, Amsalem O, Benavides-Piccione R, Delattre V, Doron M, et al. A calcium-based plasticity model for predicting long-term potentiation and depression in the neocortex. Nature Communications 2022 13:1. 2022;13: 1–19. doi:10.1038/s41467-022-30214-w
42. Tsien RW, Lipscombe D, Madison D v., Bley KR, Fox AP. Multiple types of neuronal calcium channels and their selective modulation. Trends in Neurosciences. 1988;11: 431–438. doi:10.1016/0166-2236(88)90194-4
43. Fisher RE, Gray R, Johnston D. Properties and Distribution of Single Voltage-Gated Calcium Channels in Adult Hippocampal Neurons. JOURNALOFNEUROPHYSIOLOGY. 1990;64.
44. Snutch TP, Peloquin J, Mathews E, McRory JE. Molecular Properties of Voltage-Gated Calcium Channels. 2013 [cited 28 Nov 2021]. Available: https://www.ncbi.nlm.nih.gov/books/NBK6181/
45. Eyal G, Verhoog MB, Testa-Silva G, Deitcher Y, Piccione RB, DeFelipe J, et al. Human cortical pyramidal neurons: From spines to spikes via models. Frontiers in Cellular Neuroscience. 2018;12: 181. doi:10.3389/FNCEL.2018.00181/BIBTEX
46. Rose CR, Konnerth A. Stores Not Just for Storage. Neuron. 2001;31: 519–522. doi:10.1016/S0896-6273(01)00402-0
47. Abraham WC, Bear MF. Metaplasticity: The plasticity of synaptic plasticity. Trends in Neurosciences. 1996;19: 126–130. doi:10.1016/S0166-2236(96)80018-X
48. Graupner M, Brunel N. Calcium-based plasticity model explains sensitivity of synaptic changes to spike pattern, rate, and dendritic location. Proc Natl Acad Sci U S A. 2012;109: 3991–6. doi:10.1073/pnas.1109359109
49. Redondo RL, Okuno H, Spooner PA, Frenguelli BG, Bito H, Morris RGM. Synaptic Tagging and Capture: Differential Role of Distinct Calcium/Calmodulin Kinases in Protein Synthesis-Dependent Long-Term Potentiation. Journal of Neuroscience. 2010;30: 4981–4989. doi:10.1523/JNEUROSCI.3140-09.2010
50. Manahan-Vaughan D, Kulla A, Frey JU. Requirement of translation but not transcription for the maintenance of long-term depression in the CA1 region of freely moving rats. J Neurosci. 2000;20: 8572–8576. doi:10.1523/JNEUROSCI.20-22-08572.2000
51. Tigaret CM, Olivo V, Sadowski JHLP, Ashby MC, Mellor JR. Coordinated activation of distinct Ca2+ sources and metabotropic glutamate receptors encodes Hebbian synaptic plasticity. Nature Communications. 2016;7. doi:10.1038/ncomms10289
52. Rall W. Distinguishing theoretical synaptic potentials computed for different soma-dendritic distributions of synaptic input. J Neurophysiol. 1967;30: 1138–1168. doi:10.1152/jn.1967.30.5.1138
53. Rall W, Rinzel J. Branch input resistance and steady attenuation for input to one branch of a dendritic neuron model. Biophys J. 1973;13: 648–688. doi:10.1016/S0006-3495(73)86014-X
54. Hay E, Hill S, Schürmann F, Markram H, Segev I. Models of neocortical layer 5b pyramidal cells capturing a wide range of dendritic and perisomatic active properties. PLoS Computational Biology. 2011;7. doi:10.1371/journal.pcbi.1002107

55. Dembrow NC, Spain WJ. Input rate encoding and gain control in dendrites of neocortical pyramidal neurons. Cell Reports. 2022;38: 110382. doi:10.1016/J.CELREP.2022.110382
56. Polsky A, Mel B, Schiller J. Encoding and decoding bursts by NMDA spikes in basal dendrites of layer 5 pyramidal neurons. Journal of Neuroscience. 2009;29: 11891–11903. doi:10.1523/JNEUROSCI.5250-08.2009
57. Landau AT, Park P, Wong-Campos JD, Tian H, Cohen AE, Sabatini BL. Dendritic branch structure compartmentalizes voltage-dependent calcium influx in cortical layer 2/3 pyramidal cells. Elife. 2022;11. doi:10.7554/ELIFE.76993
58. Poirazi P, Mel BW. Impact of active dendrites and structural plasticity on the memory capacity of neural tissue. Neuron. 2001;29: 779–796. doi:10.1016/S0896-6273(01)00252-5
59. Branco T, Häusser M. The single dendritic branch as a fundamental functional unit in the nervous system. Current Opinion in Neurobiology. 2010;20: 494–502. doi:10.1016/j.conb.2010.07.009
60. Poirazi P, Brannon T, Mel BW. Pyramidal Neuron as Two-Layer Neural Network. Neuron. 2003;37: 989–999. doi:10.1016/S0896-6273(03)00149-1
61. Rumelhart DE, Hinton GE, Williams RJ. Learning representations by back-propagating errors. Nature. 1986;323: 533–536. doi:10.1038/323533a0
62. Beniaguev D, Segev I, London M. Single cortical neurons as deep artificial neural networks. Neuron. 2021;109: 2727-2739.e3. doi:10.1016/J.NEURON.2021.07.002
63. Jones IS, Kording KP. Might a Single Neuron Solve Interesting Machine Learning Problems Through Successive Computations on Its Dendritic Tree? Neural Computation. 2021;33: 1554–1571. doi:10.1162/NECO_A_01390
64. Moldwin T, Segev I. Perceptron Learning and Classification in a Modeled Cortical Pyramidal Cell. Frontiers in Computational Neuroscience. 2020;14: 1–13. doi:10.3389/fncom.2020.00033
65. Mel BW. The clusteron: Toward a simple abstraction for a complex neuron. Nips. 1991; 35–42.
66. Moldwin T, Kalmenson M, Segev I. The gradient clusteron: A model neuron that learns to solve classification tasks via dendritic nonlinearities, structural plasticity, and gradient descent. Migliore M, editor. PLOS Computational Biology. 2021;17: e1009015. doi:10.1371/journal.pcbi.1009015
67. Sabatini BL, Oertner TG, Svoboda K. The Life Cycle of Ca2+ Ions in Dendritic Spines. Neuron. 2002;33: 439–452. doi:10.1016/S0896-6273(02)00573-1
68. Golding NL, Kath WL, Spruston N. Dichotomy of Action-Potential Backpropagation in CA1 Pyramidal Neuron Dendrites. 2001. doi:10.1152/jn
69. Jadi M, Polsky A, Schiller J, Mel BW. Location-dependent effects of inhibition on local spiking in pyramidal neuron dendrites. Gutkin BS, editor. PLoS Computational Biology. 2012;8: e1002550. doi:10.1371/journal.pcbi.1002550
70. Gidon A, Segev I. Principles Governing the Operation of Synaptic Inhibition in Dendrites. Neuron. 2012;75: 330–341. doi:10.1016/j.neuron.2012.05.015
71. Jadi MP, Behabadi BF, Poleg-Polsky A, Schiller J, Mel BW. An augmented two-layer model captures nonlinear analog spatial integration effects in pyramidal neuron dendrites. Proceedings of the IEEE. 2014;102: 782–798. doi:10.1109/JPROC.2014.2312671
72. Doron M, Chindemi G, Muller E, Markram H, Segev I, Eilif Muller HM, et al. Timed Synaptic Inhibition Shapes NMDA Spikes, Influencing Local Dendritic Processing and Global I/O Properties of Cortical Neurons. Cell Reports. 2017;21: 1550–1561. doi:10.1016/j.celrep.2017.10.035
73. Nishiyama M, Hong K, Mikoshiba K, Poo MM, Kato K. Calcium stores regulate the polarity and input specificity of synaptic modification. Nature. 2000;408: 584–588. doi:10.1038/35046067
74. Jo J, Heon S, Kim MJ, Son GH, Park Y, Henley JM, et al. Metabotropic Glutamate Receptor-Mediated LTD Involves Two Interacting Ca2+ Sensors, NCS-1 and PICK1. Neuron. 2008;60: 1095. doi:10.1016/J.NEURON.2008.10.050
75. O C, L T. Dendritic calcium nonlinearities switch the direction of synaptic plasticity in fast-spiking interneurons. J Neurosci. 2014;34: 3864–3877. doi:10.1523/JNEUROSCI.2253-13.2014

76. Evans R, Blackwell K. Calcium: Amplitude, Duration, or Location? Biol Bull. 2015;228: 75. doi:10.1086/BBLV228N1P75
77. O'Hare JK, Gonzalez KC, Herrlinger SA, Hirabayashi Y, Hewitt VL, Blockus H, et al. Compartment-specific tuning of dendritic feature selectivity by intracellular Ca2+ release. Science (1979). 2022;375. doi:10.1126/SCIENCE.ABM1670/SUPPL_FILE/SCIENCE.ABM1670_MDAR_REPRODUCIBILITY_CHECKLIST.PDF
78. Adelman JP, Maylie J, Sah P. Small-conductance Ca 2+-activated K + channels: Form and function. Annual Review of Physiology. 2012;74: 245–269. doi:10.1146/ANNUREV-PHYSIOL-020911-153336
79. Rodrigues YE, Tigaret CM, Marie H, O'Donnell C, Veltz R. A stochastic model of hippocampal synaptic plasticity with geometrical readout of enzyme dynamics. bioRxiv. 2021; 2021.03.30.437703. doi:10.1101/2021.03.30.437703
80. Barco A, Lopez de Armentia M, Alarcon JM. Synapse-specific stabilization of plasticity processes: The synaptic tagging and capture hypothesis revisited 10 years later. Neuroscience & Biobehavioral Reviews. 2008;32: 831–851. doi:10.1016/J.NEUBIOREV.2008.01.002
81. Frey U, Morris RGM. Synaptic tagging and long-term potentiation. Nature. 1997;385: 533–536. doi:10.1038/385533A0
82. Sun C, Nold A, Fusco CM, Rangaraju V, Tchumatchenko T, Heilemann M, et al. The prevalence and specificity of local protein synthesis during neuronal synaptic plasticity. Science Advances. 2021;7: 790–807. doi:10.1126/SCIADV.ABJ0790/SUPPL_FILE/SCIADV.ABJ0790_SM.PDF
83. Hines ML, Davison AP, Muller E. NEURON and Python. Front Neuroinform. 2009;3: 1. doi:10.3389/neuro.11.001.2009
84. Carnevale NT, M.L. Hines. The NEURON Simulation Environment. Neural Computation. 1997;1209: 1–26.
85. Yuste R, Denk W. Dendritic spines as basic functional units of neuronal integration. Nature. 1995;375: 682–684. doi:10.1038/375682a0
86. Eyal G, Verhoog MB, Testa-Silva G, Deitcher Y, Benavides-Piccione R, DeFelipe J, et al. Human Cortical Pyramidal Neurons: From Spines to Spikes via Models. Frontiers in Cellular Neuroscience. 2018;12: 1–24. doi:10.3389/fncel.2018.00181
87. Behabadi BF, Polsky A, Jadi M, Schiller J, Mel BW. Location-dependent excitatory synaptic interactions in pyramidal neuron dendrites. PLoS Computational Biology. 2012 [cited 1 Jan 2021]. doi:https://doi.org/10.1371/journal.pcbi.1002599
88. Araya R, Eisenthal KB, Yuste R. Dendritic spines linearize the summation of excitatory potentials. 2006 [cited 28 Nov 2021]. Available: www.pnas.orgcgidoi10.1073pnas.0609225103
89. Konur S, Rabinowitz D, Fenstermaker VL, Yuste R. Systematic regulation of spine sizes and densities in pyramidal neurons. Journal of Neurobiology. 2003;56: 95–112. doi:10.1002/NEU.10229
90. Cornejo VH, Ofer N, Yuste R. Voltage compartmentalization in dendritic spines in vivo. Science (1979). 2021 [cited 28 Nov 2021]. doi:10.1126/SCIENCE.ABG0501

# Supplementary Figure S1: Asymmetric transfer resistances of L5PC and ball-and-stick models

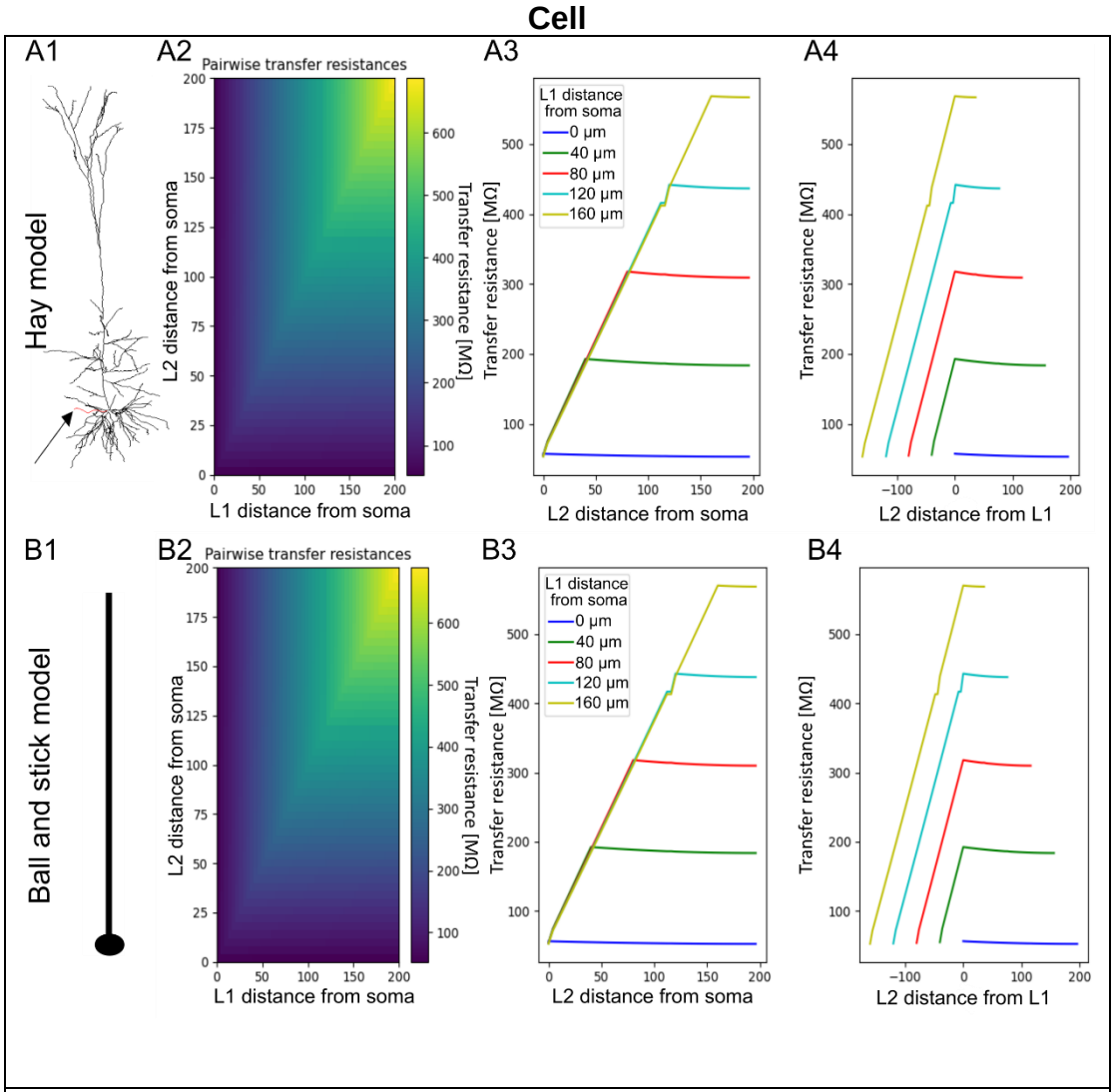


**Supplementary S1: Asymmetric transfer resistances of L5PC and ball-and-stick models**

(**A1**) Model of layer 5 pyramidal cell from [54]. Arrow indicates a dendrite modified to have the same morphological and electrical parameters as the idealized ball-and-stick model. (**A2**) Pairwise transfer resistances between each dendritic segment, presented as heatmap. L1: location 1, L2: location 2. (**A3**) Transfer resistances from selected dendritic locations (L1) to all other dendritic locations (L2) as a function of distance of L2 from the soma. (**A4**) As is A3, except L2 is depicted as a function of distance from L1, demonstrating asymmetric attenuation from each location. Negative numbers indicate L2 is more proximal than L1, positive numbers indicate L1 (**B1-B4**) Same as A1-A4, but for the ball-and-stick model used in the paper with the soma diameter adjusted to match the somatic input resistance ($R_N$) from the Hay L5PC model.

# Supplementary Figure S2. Vertical heterosynaptic sandwiching in a branched model

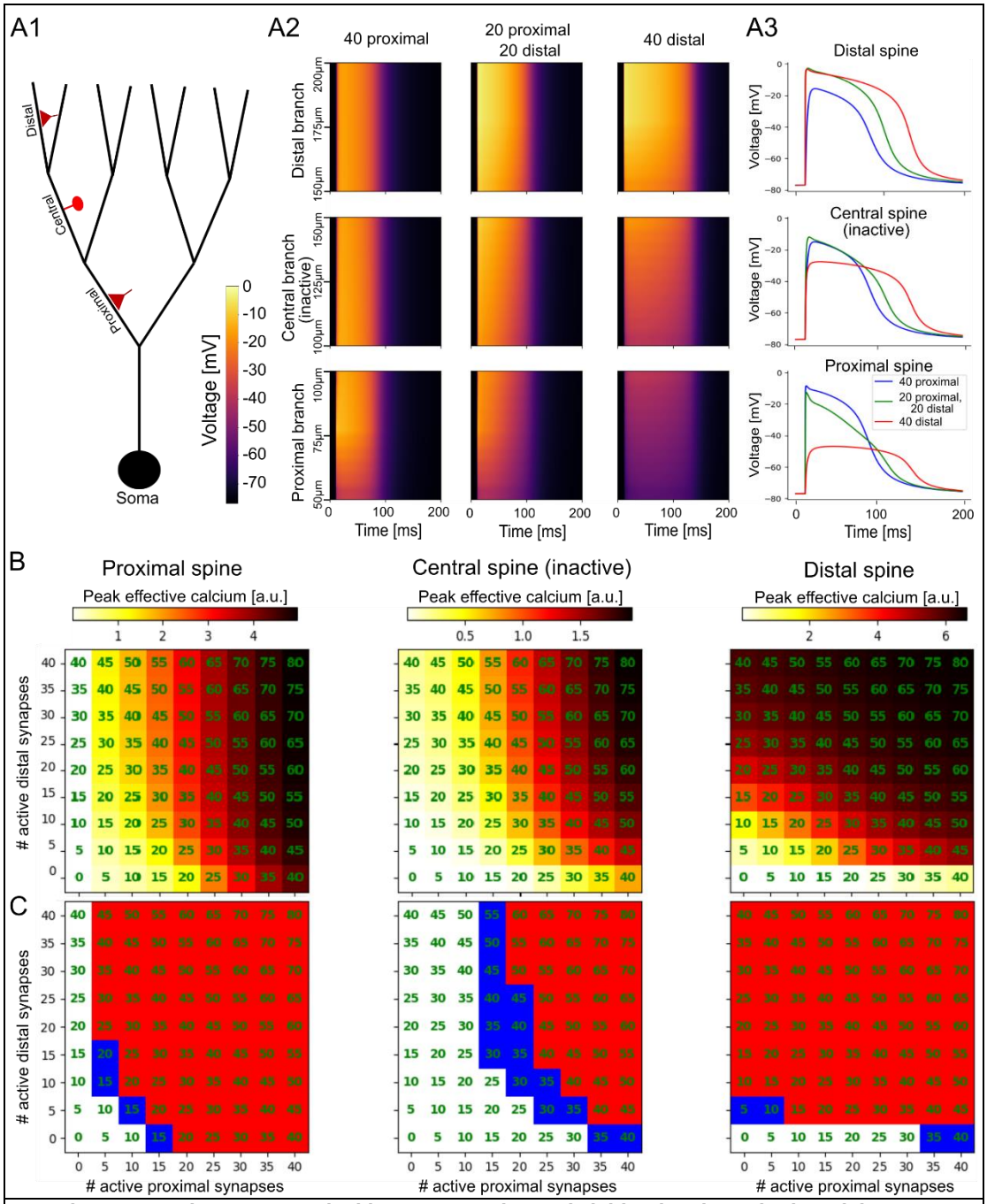


**Supplementary Figure S2. Vertical heterosynaptic sandwiching in a branched model**
**(A1)** Experiment schematic. Clusters of spines are activated at proximal (2nd layer) and distal (4th layer) branches to explore the effect on non-activated spine on a central branch (3rd layer). **(A2)** Spatiotemporal voltage profiles at the distal (top row), central (middle row), and proximal (bottom row) branches in the cases where a cluster of 40 active synapses are all placed at the center of the proximal branch (left), distal branch (right), or where two clusters of 20 synapses each are placed on the proximal and distal branches, respectively. **(A3)** Voltage traces at an exemplar spine head from the distal cluster (top), the inactive synapse on the central branch (center), or the proximal cluster (bottom) for each of the experimental protocols (40 proximal, 40 distal, 20 proximal + 20 distal). **(B)** Peak calcium at an exemplar spine on the proximal (left), central (middle) or distal (right) branches, as in Figure 5C. **(C)** Plastic effect on each spine as a function of cluster sizes (red: potentiation, blue: depression, white: no change). **B-C** same as Figure 6 in the main text.

# Supplementary Figure S3. Horizontal heterosynaptic sandwiching in a branched model

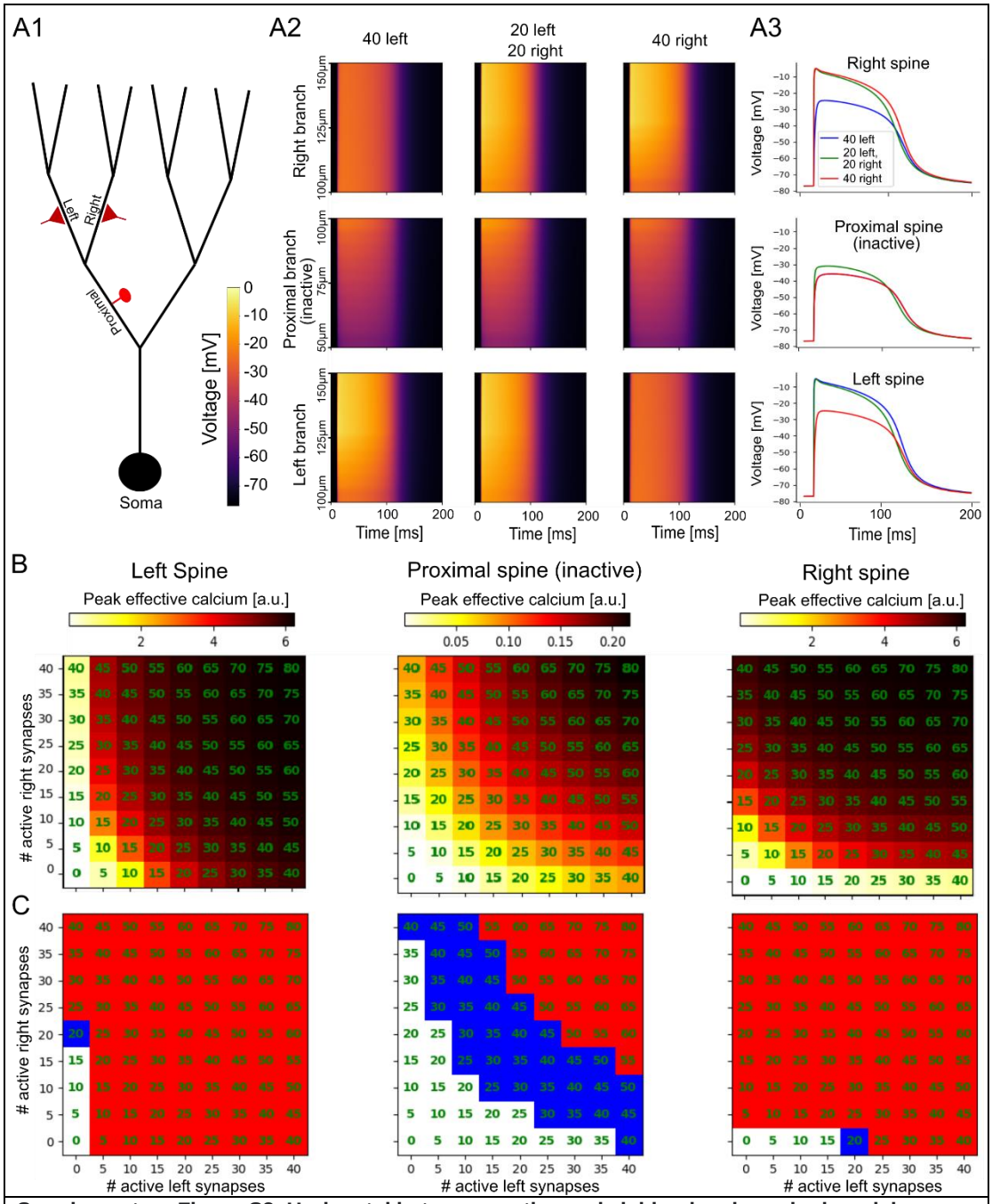


**Supplementary Figure S3. Horizontal heterosynaptic sandwiching in a branched model**
**(A1)** Experiment schematic. Clusters of spines are activated at the third branching layer on the left and right branches to explore the effect on non-activated spine on a proximal parent branch (2nd layer). **(A2)** Spatiotemporal voltage profiles at the right (top row), proximal (middle row), and left (bottom row) branches in the cases where a cluster of 40 active synapses are all placed at the center of the left branch (left), right branch (right), or where two clusters of 20 synapses each are placed on the left and right branches, respectively (center). **(A3)** Voltage traces at an exemplar spine head from the right cluster (top) proximal cluster (left) or the inactive synapse on the proximal parent branch (center) for each of the experimental protocols (40 proximal, 40 distal, 20 proximal + 20 distal). **(B)** Peak calcium at an exemplar spine on the left, proximal parent, or right branches, as in Figure 6B. **(C)** Plastic effect on each spine as a function of cluster sizes (red: potentiation, blue: depression, white: no change). [Note that to demonstrate plastic effects, calcium thresholds for plasticity used in this figure were different than in other figures, see **Methods**.) **B-C** same as Figure 6 in the main text.